Increasing Integration Density of Photonic Integrated Circuits by Employing Optimized Dielectric Metamaterial Structures

Andraž Debevc, Marko Topič, *Senior Member, IEEE*, and Janez Krč

***Abstract*—All-dielectric metamaterial structures in the role of the cladding of optical waveguides (WGs) in photonic integrated circuits (PICs) are investigated and optimized by means of numerical simulations to increase the integration density of PICs. First the role of the refractive index (material platform) on the effects of metamaterial cladding is studied. The results of a quantitative analysis show that only material platforms with a high refractive index contrast (such as existing Si or membrane InP platform) can noticeably benefit from optimized metamaterial cladding in terms of integration density. Furthermore, we perform a comprehensive optimization of the geometry of metamaterial claddings in Si platform to achieve the lowest possible gap width between cores of two adjacent WGs, while keeping the cross-talk bellow the targeted limit of −30 dB at the length of 2 mm. By doing this we can, for the first time, explicitly show how much the integration density of a PIC can be increased. We demonstrate that a metamaterial cladding can, in best case, reduce the gap width by 60% compared to Si WGs with normal cladding in case of 450 nm wide core. The wavelength dependence and sensitivity to fabrication variability are also studied, revealing a trade-off between the lowest possible integration density and usable wavelength range. We show that a sizable decrease in gap width at a wide usable wavelength range is possible, demonstrating that waveguides with metamaterial cladding have the potential to be utilized in future applications requiring a high integration density of PICs.**

***Index Terms*—All dielectric metamaterials, cross-talk, integration density, photonic integrated circuits, silicon photonics.**

I. Introduction

PHOTONIC Integrated Circuits (PICs) can perform a large number of functionalities on a single chip. By scaling down photonic components and connections the functionality of PICs can be increased and packaging costs of single components eliminated. Different material platforms to fabricate PICs have been developed, such as InP [1], Si [2], Si_3N_4 [3], SiO_2 [4], LiNbO3 [5], polymers [6] and others. Material platforms with moderate to high refractive index contrast, among them Si-based and membrane InP [7], enable denser integration of optical waveguides (WGs) and other components with sub-micrometer dimensions at telecom wavelengths [8]. However, optical cross-talk between waveguides is still one of the major factors limiting the integration density of PICs [9]. In case of Si material a minimal separation of at least one to multiple micrometers needs to be enforced between waveguiding structures [9]. Considering the typical width of a Si strip waveguide of 450 - 500 nm [10] we can assume that on average at least two thirds of a typical PIC needs to be void in order to keep cross-talk below the desired limit. Various cross-talk mitigation techniques [9], [11], [12] therefore get the attention of researchers.

All-dielectric metamaterials have been introduced as one of the possible solutions to tackle the challenge of higher integration density [13], [14]. The subwavelength structures of metamaterials offer control over refractive index of optical material in different directions, opening up a new degree-of-freedom to control light in the photonic integrated design [15]–[19]. A basic all-dielectric metamaterial structure consists of two or more periodically exchanging dielectric materials with different refractive indices. Usually one dielectric material is the same as the material of the WG core, whereas the other one is the material of the surrounding medium. Due to advanced fabrication techniques such as deep ultraviolet and e-beam lithography that are used to fabricate PICs, metamaterials can readily be integrated with PICs [20]. If the spatial period of the metamaterial is significantly smaller than the wavelength of light, the metamaterial acts as a uniform anisotropic material with different refractive indices along different lateral directions [21]. By adjusting the geometrical properties of the metamaterial subwavelength structure and the axis of polarization and light propagation we can achieve optical properties that would not be possible with conventional optical structures. Metamaterials can, in general, assist standard integrated passive optical components such as grating couplers [22], edge couplers [23], directional couplers [24], polarization rotators and splitters [25], waveguide bends [26] and many others in achieving wider bandwidth, smaller footprint, decreased losses etc. In sensing applications metamaterials can significantly increase the sensitivity of various sensor designs [27]. In many of these applications the metamaterials are designed in such a way that the geometrical features in the metamaterial structure are perpendicular to light propagation. This can effectively increase the size of the propagating optical mode. In contrast, if the features of metamaterial are in parallel to light propagation, the potential to achieve a higher confinement of the propagating mode in a waveguide

Manuscript received September 22, 2021; revised October 26, 2021; accepted October 29, 2021. Date of publication November 4, 2021; date of current version November 11, 2021. This work was supported by the Slovenian Research Agency-ARRS under Program P2-0197. The work of Andraž Debevc was supported under the Ph.D funding. *(Corresponding author: Andraž Debevc.)*

The authors are with the Faculty of Electrical Engineering, University of Ljubljana, SI-1000 Ljubljana, Slovenia (e-mail: andraz.debevc@fe.uni-lj.si; marko.topic@fe.uni-lj.si; janez.krc@fe.uni-lj.si).

Digital Object Identifier 10.1109/JPHOT.2021.3124626

This work is licensed under a Creative Commons Attribution-NonCommercial-NoDerivatives 4.0 License. For more information, see https://creativecommons.org/licenses/by-nc-nd/4.0/

can be utilized [28]–[30]. It has been demonstrated already that a waveguide with a dielectric metamaterial at the sides can exhibit a faster decay of evanescent field in the cladding region of the waveguide compared to a conventional strip waveguide [29], [31]. Adjacent waveguides with all dielectric metamaterial cladding can therefore have a considerably smaller overlap of evanescent fields compared to strip waveguides with a regular non-structured cladding, effectively lowering the cross-talk [28]. By manipulating the geometrical parameters of the metamaterial structure, the cross-talk can be further reduced, as studied in [9], [12], [28], [32].

In this paper we perform a comprehensive numerical analysis and optimization of integrated waveguide structures with all-dielectric metamaterial cladding. While previous publications [28], [32], [33] have been focused on Si platform only, we first explore, by simulations, the potential of metamaterial claddings in a broader scope of platforms and quantify the related effects. Based on the determination of coupling lengths between WGs we give directions which existing or emerging material platforms can benefit from metamaterial cladding. Further investigations and optimizations are then focused on Si material. Previous studies of Si waveguides with metamaterial cladding investigated the structures in terms of reducing the coupling length of WGs [12], [28], [32], [33], which does not necessarily lead to the highest integration density due to metamaterial structure size (related to the period and number of ribs), as well as the complex non-linear relations between geometrical parameters and coupling length. We show in this paper the optimized geometry of metamaterial structures to assure minimal separation between WGs for a certain cross-talk limit (30 dB at the WG length of 2 mm). This limit is for example even a stricter condition than suggested in [9]. This way we can explicitly demonstrate how much integration density can be increased by employing optimized metamaterial cladding. Potential radiation losses are also discussed. Furthermore, the analysis is upgraded with the study of wavelength dependency of the effects related to metamaterial claddings. This is an important aspect of the design since most applications of PICs require a reasonably wide bandwidth. Moreover, we extend the numerical simulation study to address and quantify effects of structure fabrication tolerances on the performance of metamaterial claddings. While pioneering studies [28] revealed the potential of metamaterial claddings to reduce the cross-talk between WGs, our work builds on that and provides an explicit insight into how much the integration density of PICs can actually be increased demonstrating a feasibility of this approach. Wavelength dependence and fabrication tolerance studies presented in this paper in our opinion also bring us a step further towards real applications of WGs with metamaterial cladding.

II. Theoretical Background and Methods

A. Structure Geometry

The analyzed system of two strip WGs with metamaterial cladding, presenting the main structure, is symbolically depicted in Fig. 1(a). The WG cores on top of a substrate stack (a general platform) are surrounded with subwavelength ribs from the same

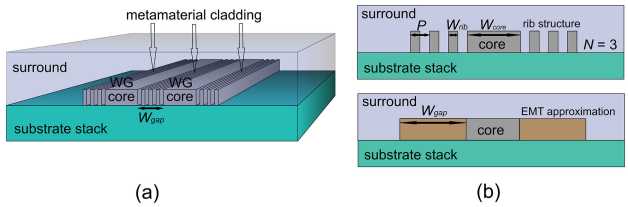

Fig. 1. (a) An example of a system of two strip WGs with a metamaterial cladding. (b) Partial cross-section of the structure with actual metamaterial cladding with three ribs on both sides (top) and the EMT approximation of the rib subwavelength structure (bottom).

material as the WG core, forming a metamaterial cladding. The gap width W_{gap} between WG cores is in our cases adjusted in such a way, that the cladding structure is symmetrical with respect to both WGs and that the gap is perfectly periodically filled with metamaterial rib structure. This means that the W_{gap} consists of a given number, N, of periods, P (where one P includes one rib and one corresponding spacing, see Fig. 1(b) (top), plus an additional spacing just before the next core, see Fig. 1(a)). The W_{gap} parameter will be used in our analysis as an indicator of integration density (smaller W_{gap}, directly means higher integration density). In Fig. 1(b) (top) the cross-section of a single WG core with metamaterial cladding is shown for simplicity, presenting a part of the entire structure of Fig. 1(a). Main geometrical parameters of metamaterial cladding are defined in the figure: the period P, the width of a rib W_{rib}, the fill factor $ff = W_{rib} / P$ and the number of ribs N.

B. Theoretical Background

As mentioned, the metamaterial cladding exhibits anisotropy in refractive index due to its subwavelength structure. In case of a regular structure of the strip WG system the total internal reflection (TIR) condition at the interface of two isotropic materials dictates that the refractive index of the incident (WG core) medium needs to be higher than the refractive index of the second medium (WG cladding). In case of the structure with metamaterial cladding the second medium can be considered as anisotropic, exhibiting a different refractive index in the direction perpendicular to the interface than in the direction parallel to the interface. The TIR condition depends only on one component of refractive index of the second medium – relaxed TIR condition [30]. In case of TM-polarized light the refractive index of the incident medium needs to be higher than the refractive index of the second medium perpendicular to the interface and in case of TE-polarized light the refractive index of the incident medium needs to be higher than the refractive index of the second medium in parallel to the interface. This means that for integrated strip WGs with an anisotropic cladding, the TIR condition for TE-like modes depends only on the perpendicular refractive index of the cladding. The parallel component of refractive index of the cladding can therefore be arbitrarily increased while maintaining the TIR condition assuring that the mode remains guided in the WG. As a consequence the evanescent fields extending into the cladding are confined closer to WG core [29], [30], leading to a smaller cross-talk. By optimizing the actual geometry of

the metamaterial the cross-talk and consequently the distance between two adjacent WGs can be reduced.

Linked to the cross-talk we will first focus on the coupling length parameter, L_x which is defined as the length at which all the power from the excited WG couples to the adjacent WG. Supermode method [34] is used to calculate the Lx from the difference of effective refractive indices (n_{eff}) of the symmetric and antisymmetric modes of the system of two WGs, following equation 1, where λ_0 is the wavelength of light in vacuum and

$$L_x = \frac{\lambda_0}{2\,\Delta n_{eff}} \tag{1}$$

Δn_{eff} is the absolute effective refractive index difference of a symmetric and antisymmetric mode. In case of a WG with isotropic cladding, the n_{eff} of the symmetric mode is always larger than that of the antisymmetric mode. This is called a trivial coupling regime. In case of a WG with anisotropic cladding however, a so called non-trivial coupling regime can be achieved where the n_{eff} of the antisymmetric mode is larger than that of the symmetric mode. This only happens in a limited region of the parameter space. At the transition from a trivial into a non-trivial coupling regime there exists a certain combination of parameters at which Δn_{eff} is zero. This means that there is a singularity in L_x where it approaches infinity and the cross-talk is completely suppressed [33]. This exceptional coupling point can be reached by tuning the components of the refractive index of anisotropic side cladding. Also the points around this singularity point exhibit high L_x values. In case of a real rib subwavelength metamaterial structure this region of large L_x can be achieved by tuning the geometrical parameters (*ff, P, N*). By making use of this effect the coupling length can be orders of magnitude higher (for a comparable W_{core} and W_{gap}) than that achieved by only employing a metamaterial cladding to increase the evanescent field decay in the cladding such as in [28].

Another approach to mitigate cross-talk is to introduce an asymmetry into the system of WGs in order to achieve phase mismatched WGs. This can be done either by employing different core widths [9], or by introducing asymmetry into the cladding [35]. Such an approach in combination with metamaterial cladding could possibly yield even better results in terms of integration density, however it would introduce additional complexities into the design since different propagation constants of WGs would need to be accounted for. In this paper we therefore focus only on symmetric structures, since we think they present a more universal solution.

C. Methods

The geometry of the metamaterial cladding can be considered in the analysis in two ways: as it is (rigorous approach) or it can be approximated, in a simplified approach, with a homogeneous anisotropic material by employing Effective Medium theory (EMT) [21] as shown in Fig. 1(b) (bottom). When infinitesimally small period of metamaterial structure is assumed, the fill factor is the only geometrical parameter (besides refractive indices) that governs the properties and anisotropy of the structure.

In the EMT approximation the parallel and perpendicular refractive indices (with respect to the WG) of the substitute homogeneous material can be calculated from equations 2, where n_{core} is the refractive index of a higher index constituent material (core material) and $n_{surround}$ is the refractive index of a lower index constituent material (surrounding material) and *ff* is the area fill factor.

$$n_{||} = \sqrt{n_{core}^2\, ff + n_{surround}^2\, (1-ff)}$$
$$n_{\perp} = \sqrt{\frac{1}{\frac{ff}{n_{core}^2} + \frac{1-ff}{n_{surround}^2}}} \tag{2}$$

For the Si platform, which was used in detailed analysis we used Lorentz model to approximate the refractive index of Si [36]. The refractive index of SiO_2 was chosen to be constant (1.47) in the simulated wavelength range.

As a simulation tool a commercially available software COMSOL [37] was employed to perform a 2-D Finite Element Method based mode analysis in the cross-section of WG systems to find propagating modes and their effective refractive indices. We calculate it by means of supermode theory as described in previous paragraphs. This approach was used in both cases, when analyzing metamaterial cladding with the actual geometry of rib subwavelength structure as well as when applying the EMT approximation. The analysis of WGs with metamaterial cladding shown in next sections is made only for TE modes, since the metamaterial cladding structure (as shown in Fig. 1) does not carry the potential to reduce the cross-talk for TM polarized modes as has been reported already in [28].

III. Results and Discussion

A. Material Refractive Index Variation

Results of variation of material refractive indices of the WG core and the surrounding are presented first. This way we are able to demonstrate the effects related to metamaterial cladding for different material platforms. In this general study the EMT method was employed, where infinitesimally small period of the metamaterial structure, compared to light wavelength was assumed. Besides scanning different refractive indices of the core and the surrounding materials, we simultaneously varied the metamaterial structure in terms of *ff* parameter. The simulations were performed at the chosen wavelength of 1550 nm (central c-band wavelength, defined in vacuum). SiO_2 layer (infinite thickness assumed in simulations) was considered as the top layer of the substrate in all the cases.

Results of the analysis are presented in Fig. 2. L_x parameter is monitored as a function of different combinations of the core and the surround material for a selected WG structure with metamaterial cladding. Refractive indexes of selected optical materials most often used in photonic integration are marked by dashed lines on the plots. A broader range of investigation enables us to quantify the effects related to metamaterial claddings also for alternative and novel material platforms. Let us first elaborate on the results presented in Fig. 2(a) and 2(c) where the core refractive index n_{core} is changed from 2.0 to 3.7 (vertical axis) and the *ff* from 0.1 to 0.9 (horizontal axis). Air with $n = 1$ (a) and SiO_2 with $n = 1.47$ (c) are considered as the top surrounding material (represented by blue colour in Fig. 1),

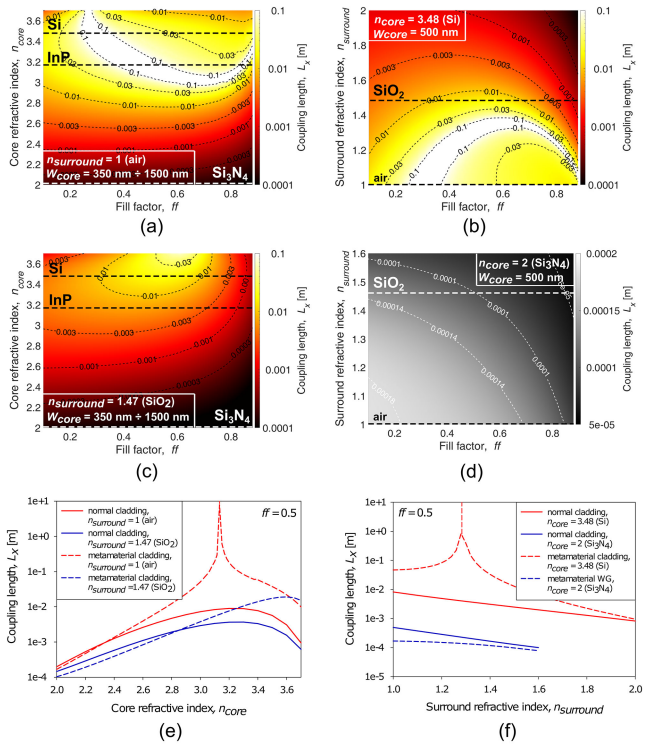

Fig. 2. Coupling length of WGs as a function of fill factor and refractive indices of constituent materials for TE mode. EMT of the metamaterial cladding was used in these simulations. Refractive indexes of Si, InP, Si_3N_4 and SiO_2 are marked on the plots with dashed lines. (a) Refractive index of surround material is fixed to 1 (air) and the ff and the refractive index of the core material are varied. The width of waveguide core is linearly adjusted with the change of refractive index in order to ensure light propagation and single-mode condition (see main text). (b) Refractive index of core material is fixed to 3.48 (Si) and the ff of metamaterial and the refractive index of the surround material are varied. The width of the waveguide core is fixed to 500 nm in this case. (c) Refractive index of surround material is fixed to 1.47 (SiO_2) and the ff of metamaterial and the refractive index of the core material are varied. The width of waveguide core is linearly adjusted with the change of refractive index. (d) Refractive index of the core material is fixed to 2 (Si_3N_4) and the ff of metamaterial and the refractive index of the surround material is varied. The width of the waveguide core is fixed to 1500 nm in this case.

the bottom surrounding material is SiO_2, as mentioned. The corresponding values of L_x are colour-coded (see legend). The W_{gap} parameter is fixed to 700 nm in these cases. The vertical thickness of the waveguiding layer and metamaterial structure was set to 220 nm (in all simulations). However, the width of the core (W_{core}) was linearly adjusted from 450 nm at $n_{core} = 3.7$ (Si) to 1500 nm at $n_{core} = 2$ (Si3N4) to consider the single mode condition in relation to n_{core} variation. A general observation from these results is that L_x values around the maximal regions are significantly higher in case of air surrounding (Fig. 2(a)) compared to SiO_2 (Fig. 2(c)). In both cases a trend can be seen that L_x increases with higher refractive index of the core material, however, a decrease in L_x can be observed for the air case at $n_{core} > 3.4$ and $ff > 0.4$. In case of air as the surrounding material we can observe a narrow region at high values of n_{core} where L_x increases significantly (unlimitedly as shown later in Fig. 2(e)). This effect at certain combinations of n_{core} and ff does not occur in case of SiO_2 surround. Before discussing the obtained results further, we introduce and describe the plots of Fig. 2(b) and Fig. 2(d).

In Fig. 2(b) and 2(d) n_{core} is fixed to 3.48 (Si) (b) and 2.0 (Si_3N_4) (d) while $n_{surround}$ is varied (vertical axis). The core width is fixed to 500 nm and 1500 nm in case of Si and Si_3N_4 material, respectively. In case of Si core, we vary the $n_{surround}$ from 1 to 2 and in case of Si_3N_4 core only from 1 to 1.6, since at higher values the condition for total reflection of the mode is violated. We can observe that in case of Si core the L_x decreases with higher values of $n_{surround}$. A narrow region can be seen at small values of $n_{surround}$ where the L_x increases significantly (unlimitedly as shown later in Fig. 2(f)). In case of Si_3N_4 core the L_x is significantly shorter due to a lower refractive index contrast between n_{core} and $n_{surround}$. Similar to the case of Si core, the L_x also decreases with higher values of $n_{surround}$, however, the change is significantly smaller (note that the colour-code is changed in this case for better visibility). No singularity can be observed in this case.

In Fig. 2(e) and 2(f) selected vertical cross-sections (at $ff = 0.5$) from Fig. 2(a)–(d) are shown to additionally identify the dependency of L_x on n_{core} and $n_{surround}$, respectively. In addition, L_x curves corresponding to the WGs with a normal cladding are added for comparison. Please note that n_{core} and $n_{surround}$ are now represented on horizontal axes, whereas the vertical axes are simulated L_x values. In Fig. 2(e) we can observe that by n_{core} variation and air surround, L_x values of WG structures with metamaterial cladding are higher compared to that of WGs with normal cladding, when n_{core} is higher than 2.4. In case of SiO_2 surround this happens when n_{core} is higher than 2.9. The difference in L_x values are also significantly smaller compared to air surround. In case of $n_{surround}$ variation and Si core, we can see that L_x of WGs with metamaterial cladding is larger compared to that of WGs with normal cladding when $n_{surround}$ is between 1 and 2. The increase in L_x is the biggest when $n_{surround}$ is below 1.4. In case of Si_3N_4 core the situation is reversed and the L_x of WGs with metamaterial cladding drops below the L_x of WGs with normal cladding.

We can observe that in case of air surround (Fig. 2(a) and Fig. 2(c)) there exist certain combinations of n_{core} and ff where L_x rises dramatically. This effect has already been introduced in Section II.B. Since simulations are limited by a finite mesh, we cannot obtain infinite *Lx.* We can however detect the transition point of a symmetric and antisymmetric mode. In Fig. 2(e) and 2(f) we indicate this singularity with a dashed vertical line to mark the infinite L_x in this point. Note that, when relevant, the same approach will be taken in other figures of this paper as well.

Presented results in Fig. 2 reveal that a high refractive index contrast between the core and surround material is crucial for efficient performance of metamaterial cladding in WG structures. The refractive index contrast of air (1) and Si_3N_4 (2.0), for example, is too low for the metamaterial cladding to increase the coupling length. It can be observed in Fig 2(e) and 2(f) that there exist regions where L_x corresponding to the structure with metamaterial is even lower than that of WGs with normal cladding (dashed curves below the full ones). In case of Si core ($n_{core} = 3.48$) the refractive index contrast is sufficiently high

so that the L_x can be increased with air surround ($n_{surround} = 1$) as well as SiO_2 surround ($n_{surround} = 1.47$). The infinite L_x however, can only be achieved in case of the surround refractive index below 1.4. Presented results emphasize the importance of a high refractive index contrast platform such as Si or membrane InP for the performance of WGs with metamaterial cladding. WGs fabricated on low and medium refractive index contrast platforms such as SiO_2, polymers, Si_3N_4 and conventional InP will not benefit from metamaterial cladding.

B. Optimization of Metamaterial Structure

In previous section we scanned different materials (refractive indices) for best operation of metamaterial structures in the role of the WG cladding. Results showed that one of the promising platforms in this respect is Si (with air as the top surrounding material). Our further research and optimization is focused on this material platform, silicon on insulator (SOI), where air was considered as the top surrounding material. Rigorous simulations, where the exact geometry of the metamaterial structure is assumed, were performed here. Besides *ff*, other geometrical parameters of the metamaterial structure were varied and optimized.

In order to quantify the potential increase in integration density, a limitation for the cross-talk at a certain WG length was set: in our case we selected the value of -30 dB at the WG length of 2 mm. The selected condition requires the L_x of (at least) 0.1 m. In our further analysis we included strip WGs with four different widths, $W_{core} = 350$, 400, 450 and 500 nm. The thickness of the WGs was 220 nm in all cases. Considering the cross-talk condition we calculated the corresponding minimal gap between the WG cores (W_{gap}). We consider W_{gap} as an indicator of integration density on a chip. In case of a metamaterial cladding, this gap is filled with a metamaterial subwavelength structure (ribs and gaps). When adjusting the geometry of this structure we are limited by minimal feature size of the selected fabrication process. We choose this limit to be 50 nm, as this is considered to be the limit of electron-beam lithography [15]. As a reference we first simulated WG structure with normal cladding (air as top surround in this case) and determined minimal W_{gap}. The obtained values are $W_{gap} = 1.974$ μm, 1.466 μm, 1.251 μm and 1.130 μm for W_{core} of 350 nm, 400 nm, 450 nm and 500 nm, respectively.

We optimized the metamaterial cladding in terms of high integration density to obtain minimal W_{gap} with different metamaterial structures: different values of *P* and *N* of Si ribs between strip WG cores, variation of *ff* parameter while keeping the cross-talk bellow the selected reference value of –30 dB (at the length of 2 mm). For each combination *ff* was varied from 0.1 to 0.9. In simulated structures the values of W_{gap} are defined by *P*, *N* and *ff* so that the gap between WGs was always perfectly periodically filled with the metamaterial structure. For a chosen combination of *P* and *N*, W_{gap} therefore linearly decreases when increasing *ff*.

First we present the results of L_x for selected parameters of metamaterial structures (*ff, N, P* and consequently W_{gap}) for the Si platform. Then we will proceed with evaluation of integration density linked to minimal W_{gap}.

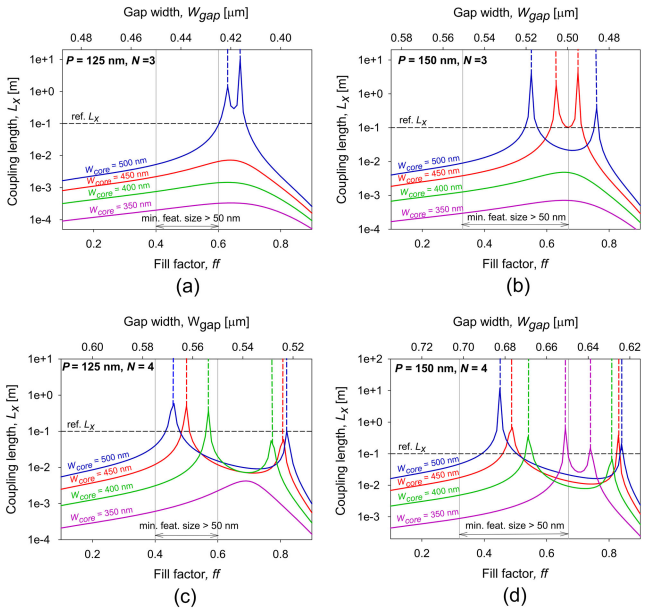

Fig. 3. Coupling length of WGs as a function of fill factor of metamaterial structures for the TE mode. By changing the *ff* parameter (bottom horizontal axis) it has to be noted that also the gap width W_{gap} (top horizontal axis) is changed, as the *ff* value affects the width of the (last) spacing as well ($W_{gap} = N$ x P + spacing width). The dashed horizontal line signifies the coupling length dictating –30 dB of cross-talk. Gray vertical lines signify the limits within which the selected minimal-feature-size condition (50 nm) is satisfied. The results are shown for two selected fixed periods of 125 nm and 3 ribs of metamaterial (a), a period of 150 nm and 3 ribs of metamaterial (b), a period of 125 nm and 4 ribs of metamaterial (c) and a period of 150 nm and 4 ribs of metamaterial (d).

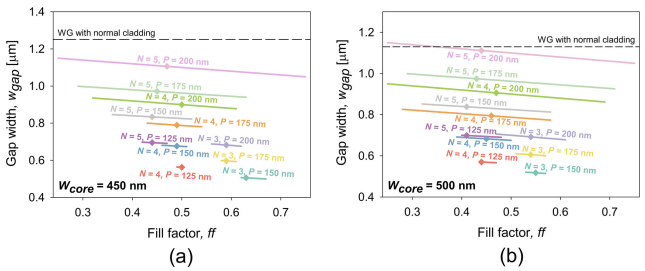

Fig. 4. The gap width W_{gap} as a quantitative indicator of integration density, as a function of of fill factor of specified metamaterial structures. Results are shown for different spatial periods and numbers of ribs. Points on the graph depict maximal coupling lengths, lines are drawn only for the span of fill factors when the coupling length is longer than 0.1 m. Reference lines depicting W_{gap} of WGs with normal cladding are added to illustrate the increase in integration density. Results are shown for a W_{core} of 450 nm (a) and 500 nm (b).

In Fig. 3(a)–(d) results of simulations for selected combinations of $P = 125$ nm and $N = 3$ (a), $P = 150$ nm and $N = 3$ (b), $P = 125$ nm and $N = 4$ (c) and $P = 150$ nm and $N = 4$ (d) are shown. We only show the most representative results with selected combinations of parameters where the effect of metamaterial cladding is the most pronounced. Results of more tested combinations of parameters are gathered later in Fig. 4. Reference lines of $L_x = 0.1$ m are added. In this analysis Si WGs with four core widths were included, $W_{\mathrm{core}} = 350$, 400, 450 and 500 nm. In all graphs we can observe that there exist certain combinations of parameters where the L_x is above the targeted reference L_x value or even it rises dramatically due to

aforementioned singularities described in section II.B. We can see that there is a limited band of *ff*s around the singularity where the L_x is larger than the reference value. Vertical lines on the graphs depict the limits of the area where the minimal feature size of the metamaterial structure is larger than the chosen limit of 50 nm. To ensure that the structure can be fabricated with current state-of-the-art fabrication processes such as e-beam, the parameters need to be chosen in a way that the peak of L_x appears in between those limits. In case of of $P = 125$ nm and $N = 3$ there is no singularity for $W_{core} = 350$ nm, 400 nm and 450 nm and the L_x does not exceed the reference value. Two peaks where L_x exceeds the reference level can be observed in case of $W_{core} = 500$ nm, however they only occur when the metamaterial structure has feature sizes smaller than 50 nm. In case of $P = 150$ nm and $N = 3$, the peaks of coupling length exceeding the reference level can be observed at two widest cores. Left peaks can be chosen so that the minimal feature size condition is satisfied. In case of $N = 4$ there exist peaks of coupling length exceeding the reference level at both shown periods ($P = 125$ nm and $P = 150$ nm). The peaks can be chosen so that the minimal feature size condition is satisfied. In case of $P = 150$ nm the peaks can be observed for all four core widths.

To find more possible structures with L_x exceeding the selected reference level we tested metamaterial cladding with different combinations of spatial period P (125, 150, 175 and 200 nm) and number of Si ribs between WG core N (2, 3, 4 and 5). Furthermore, from these results we highlighted the W_{gap} parameter as a quantitative indicator affecting the integration density. From this point on we focus only on two core widths ($W_{core} = 450$ nm and $W_{core} = 500$ nm) since they present typical values for strip WGs in most Si integration platforms. In Fig. 4 we gathered the results of many tested parameter combinations, all yielding L_x values above the chosen reference level for the case of $W_{core} = 450$ nm (a) and $W_{core} = 500$ nm (b). The graphs show W_{gap} as a function of *ff* for all these combinations of the parameters. The combinations of number of ribs in between WG cores and period are marked for each case in the graphs. The symbols on the graphs depict peak (singularity) positions and the lines depict the spans of values where L_{x} is above the reference level. The required gap width of WGs with normal cladding is marked on the plots to illustrate how much the gap width is reduced by employing the metamaterial cladding. We only show results for structures with minimal feature sizes larger than 50 nm to ensure they are amenable for fabrication with electron-beam lithography [15]. In our analysis we found 7 possible structures with W_{gap} smaller than 0.8 μm (this value corresponds to minimal W_{gap} for normal cladding) at both core widths. These are the cases with significantly higher integration density compared to WGs with normal cladding. The minimal achieved W_{gap} was 0.50 μm in case of 450 nm wide core and 0.51 μm in case of a 500 nm wide core. Compared to waveguides with normal cladding this represents a 60% and 55% decrease in minimal W_{gap} in case of $W_{core} = 450$ nm and $W_{core} = 500$ nm respectively. This means an improvement in the integration density of 45% and 38% in case of $W_{core} = 450$ nm and $W_{core} = 500$ nm respectively. A general trend can be observed that the cases with a smaller W_{gap} exhibit a narrower range of suitable *ff* values where the crosstalk stays below the reference level. We also tested structures with two ribs ($N = 2$), but there was no case where L_x would exceed the reference value, since the singularity effect did not occur. Since we only show results for a discrete set of periods, the minimal achieved W_{gap} is not exactly a theoretical global minimum of the optimization problem, however we can assume that the achieved result is not far from it. This is because we cannot achieve a singularity when accounting for fabrication limitations in case of $N = 3$ and $P = 125$ nm, so it is safe to assume that the W_{gap} below around 0.45 μm is not possible. Structures with W_{gap} close to that value have singularities very close to min. feature size limit, which is not desired. Structures in case of $N = 3$ and $P = 150$ nm exhibit singularities with some margin of *ff*s with respect to min. feature size limit and can therefore be seen as more practical.

Note that structures with larger periods ($P = 200$ nm) exhibit larger minimal feature sizes of around 100 nm making them amenable for fabrication also with state-of-the-art wafer-scale optical lithography [15].

With respect to integration it is also important to address the losses. Sidewall scattering losses are an important effect originating from fabrication imperfection that is limiting the performance of WGs, however it has been shown that the scattering losses of WGs with metamaterial cladding are comparable or only slightly higher than those of WGs with normal cladding [28].

Another important aspect of integration density are bend losses limiting the minimal bend radii of WGs. We performed 3-D FEM simulations to obtain bend losses of WGs with normal cladding and WGs with metamaterial cladding for the case of a 90° bend and 5 mm bend radius. The simulations inherently accounted for both radiative losses as well as mode mismatch losses at the transition from straight to bent WG. However, the scattering losses due to imperfect surfaces are not included in simulations. We tested structures with minimal W_{gap} for both core widths. Simulations revealed that WGs with metamaterial cladding exhibit slightly increased bend losses compared to WGs with normal cladding – by 0.0034 dB and 0.0038 dB in case of $W_{core} = 450$ nm and 500 nm respectively. This however, represents less than 0.1% of power loss per bend compared to WGs with normal cladding in both cases. Our simulations also confirmed that for WGs with narrower cores ($W_{core} = 350$ nm) exhibiting stronger evanescent field in the cladding, the bend losses of WGs with metamaterial cladding can even be smaller than the bend losses of WGs with normal cladding. This has been previously also experimentally demonstrated in [28]. Since the performance of WGs in terms of bend losses is not significantly impaired by employing a metamaterial cladding, we predict that stricter constraints with regard to minimal bend radii do not need to be imposed.

Since the performance of metamaterial cladding depends on refractive indexes of constituent materials (as shown in chapter III.A.) and since the dependence is strongly nonlinear around optimal points (singularities), it is expected that temperature will have a noticeable impact on the performance. Applications would therefore require precise temperature control of the whole chip, or micro-heaters would need to be integrated with the WGs

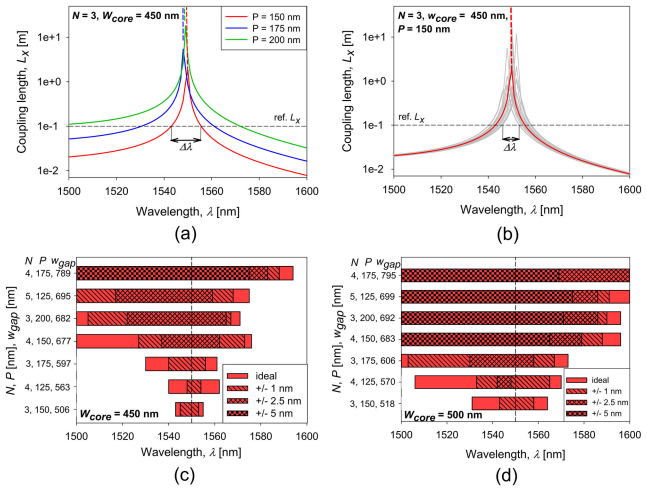

Fig. 5. (a) Coupling length in dependence of wavelength of light at three different periods of metamaterial structure (P = 150, 175 and 200 nm) with 3 ribs. Dashed line depicts the reference coupling length of 0.1 m above which the cross-talk condition is satisfied. $\Delta\lambda$ depicts the wavelength range where this condition is satisfied. (b) Coupling length in dependence of wavelength of light for the same structure while accounting for fabrication variabillity. Red line plot shows the coupling length of ideal (targeting) structure and grey line plots show coupling lengths of randomly generated structures within a chosen tolerance of $+/-$ 1 nm of every lateral edge of the structure. (c) and (d) usable wavelength range of all the optimized structures with Wgap smaller than 0.8 um. Results are shown for the ideal case and fabrication tolerance of $+/-$ 1 nm and $+/-$ 2.5 nm for Wcore = 450 nm (c) and Wcore = 500 nm (d).

to precisely tune the central wavelength, which is a standard procedure in Silicon photonics [38]. Since already a slight change in refractive index of one of the constituent materials can noticeably change the coupling length around the singularity, the effect could in principle be used for optical switching as an alternative application.

C. Wavelength Range and Sensitivity to Fabrication Tolerances

Up to this point the simulations were carried out for a single wavelength of 1550 nm (specified for vacuum). To test the wavelength dependence of the effects related to metamaterial cladding we performed a wavelength sweep from 1500 nm to 1600 nm for every optimized parameter combination from Fig. 4. In Fig. 5(a) we show wavelength dependency of L_x just for the cases corresponding to $N = 3$, $W_{core} = 450$ nm at three different periods, P = 150 nm, 175 nm and 200 nm. We can see that the peaks of L_x are at 1550 nm, since that was the wavelength at which we optimized the structures. Minor deviations of the peak positions are attributed to a finite mesh when optimizing the structures with respect to *ff*. From these results we can determine the usable wavelength range ($\Delta\lambda$), where L_x is longer than the selected reference level. It can be seen that the range increases with longer periods as well as wider WG core. The smallest $\Delta\lambda$ occurs in case of structures with the smallest gap width ($\Delta\lambda$ = 12 nm for $W_{core} = 450$ nm and $\Delta\lambda = 31$ nm for $W_{core} = 500$ nm). This indicates that there exists a trade-off between usable wavelength range and gap width (integration density).

In the last part of the paper we investigate how the fabrication tolerances affect the optical properties of the analyzed structures. In particular, small deviations in lateral dimensions of the metamaterial features are under the scope. To account for fabrication variability, we assumed that the position of every edge of the structure can be at a random position within a chosen tolerance. This covers a wider range of possible fabrication imperfections than if we only account for a change in linewidth. To ensure the validity of the supermode theory approach, we enforced the symmetry of the structure. It is expected that such approach yields a worst case scenario, since asymmetrical structures typically exhibit longer coupling lengths. For each optimized structure we generated 20 randomly modified structures with a uniform distribution of edge deviation.

We limit our investigation of sensitivity to fabrication imperfections to deviations in lateral dimensions of fabricated structures. We performed a parameter variability analysis of optimized structures. Fig. 5(b) shows selected results of this analysis for the case of $N = 3$, $W_{core} = 450$ nm and $P = 150$ nm. Red line plot represents the wavelength dependency of an ideal (as designed) structure and grey line plots are results generated by fabrication variability analysis where lateral edges of the structure are randomly positioned within a small chosen tolerance $+/-$ 1 nm. We can see that varying the structure in this range does not significantly change the shape of wavelength dependency of L_x. Simulation showed that these small structure variations do not significantly affect the evanescent field decay in the cladding region of waveguides, however, they can introduce a shift of wavelength at which the propagating constants of a symmetric and antisymmetric mode are equal. This means that the peaks of L_x can appear at different wavelengths within a certain margin. By accounting for this margin, the $\Delta\lambda$ effectively shrinks. In case of the structure shown in Fig. 4(b) the $\Delta\lambda$ is reduced from 12 nm (ideal case) to 8 nm, considering the aforementioned tolerance range of $+/-1$ nm.

The tolerance study was applied to all optimized structures with W_{gap} smaller than 800 nm. Often the application will require a certain wavelength range of operation and the fabrication process will have limitations introducing geometrical variations of fabricated structures. To present the trade-off between integration density, usable wavelength range and sensitivity to fabrication variability more systematically, we show horizontal bar charts of wavelength range for all the optimized structures with the W_{gap} below 0.8 μm (Fig. 5(c) and 5(d)). Results for $\Delta\lambda$ are shown for the ideal case as well as for the case of three fabrication tolerances: $+/-$ 1 nm, $+/-$ 2.5 nm and $+/-$ 5 nm. The full width of a bar represents $\Delta\lambda$ in the ideal case, the width of a single hatched bar represents $\Delta\lambda$ in case of +/- 1 nm tolerance, the width of a double hatched bar represents $\Delta\lambda$ in case of +/- 2.5 nm tolerance and a chessboard patterned bar represents $\Delta\lambda$ in case of +/- 5 nm tolerance. Such fabrication tolerances are strict, yet achievable with current state-of-the-art fabrication processes [39].

Results indicate that the structures with narrower W_{gap} are in general exhibiting narrower wavelength ranges and are also more sensitive to fabrication variability. For the tolerance +/- 1 nm, all the structures exhibit a wavelength range where cross-talk can

be reduced bellow the reference level, even in case of structures with the smallest W_{gap} for both cases, $W_{core} = 450$ nm and 500 nm. The already narrow wavelength ranges of these structures in the ideal case however, get even narrower by accounting for fabrication variability with +/- 1 nm. In case of variation in the range of +/- 2.5 nm, the three structures with the smallest W_{gap} cannot reliably reduce the cross-talk bellow the reference level, when $W_{core} = 450$ nm even only at the central wavelength. In case of $W_{core} = 500$ nm this happens only for one structure. Two structures with reasonably wide wavelength range at assumed fabrication variability +/- 2.5 nm are $N = 4$, $P = 150$ nm and $W_{gap} = 677$ nm with $\Delta\lambda = 25$ nm in case of $W_{core} = 450$ nm and $N = 3$, $P = 175$ nm and $W_{gap} = 606$ nm with $\Delta\lambda = 28$ nm in case of $W_{core} = 500$ nm. In both cases the W_{gap} is still reduced by 46% compared to waveguides with normal cladding representing a 34% and 32% increase in integration density for $W_{core} = 450$ nm and 500 nm respectively. Structures with wider gap widths are exhibiting wider $\Delta\lambda$ up to over 100 nm in case of $W_{core} = 500$ nm, $N = 4$, $P = 175$ nm and $W_{gap} = 795$ nm, however the gap width is reduced by only 30% in this case which represents a 21% increase in integration density. In case of variation in the range of +/- 5 nm and $W_{core} = 450$ nm only one structure with the widest W_{gap} exhibits a usable wavelength range. In case of $W_{core} = 500$ nm usable wavelength range exist in case of 4 structures with the widest W_{gap}. The W_{gap} is therefore reduced by at most 37% and 40% for $W_{core} = 450$ nm and 500 nm respectively. This represents a 27% increase in integration density for both core widths. $\Delta\lambda$ in these two cases is relatively wide: > 75 nm and > 64 nm for $W_{core} = 450$ nm and 500 nm respectively. A general trend can be observed that WGs with $W_{core} = 500$ nm exhibit wider wavelength range compared to WGs with $W_{core} = 450$ nm in case of ideal structures as well as when we account for fabrication variability.

IV. Conclusion

In this paper we showed the results of a numerical study of integrated optical waveguides with all-dielectric metamaterial cladding. We tested the capability of metamaterial cladding to reduce the cross-talk between waveguides for different material refractive indices (platforms). Results confirmed that a high refractive index contrast is crucial for desirable performance. This makes the platforms, such as Si most promising to further increase the integration density of the components. Based on these findings we optimized Si WGs in terms of minimal gap between WG cores to stay below the chosen reference cross-talk level of –30 dB at WG length of 2 mm. We assumed a minimal feature size of optimized structures to be 50 nm to ensure that they are amenable for fabrication. This way we were able to quantitatively demonstrate the capability of metamaterial cladding to increase integration density of PICs. We have shown that in the best case the gap width can be reduced by 60% in case of $W_{core} = 450$ nm and 55% in case of $W_{core} = 500$ nm compared to waveguides with normal cladding. This represents a sizable increase in integration density of Si WGs. Furthermore, we studied the wavelength dependence of optimized metamaterial structures as well as their sensitivity to fabrication variability. A general trend was observed that structures with the lowest achieved gap width tend to exhibit the narrowest wavelength range and the highest sensitivity to fabrication variability. This trade-off needs to be taken into account when designing waveguides with metamaterial cladding. For example, a compromise can be drawn for a structure with a reasonably wide wavelength range $\Delta\lambda = 25$ nm ($W_{core} = 450$ nm, variation of +/- 2.5 nm) and a still significant decrease in gap width of 46% compared to WGs with normal cladding. If application requires a wider wavelength range, or if fabrication tolerance is larger, another structure can be chosen exhibiting a decrease in gap width of 37%, which still represents a noticeable increase in integration density. All in all waveguides with all-dielectric metamaterial cladding can pave the way towards chips with a higher number of components on the same surface area in case of applications requiring a large numbers of waveguides, without significantly compromising the performance.

References

[1] M. Smit, K. Williams, and J. van der Tol, "Past, present, and future of inp-based photonic integration," *APL Photon.*, vol. 4, no. 5, May 2019, Art. no. 050901, doi: 10.1063/1.5087862.

[2] A. Novack *et al.*, "Progress in silicon platforms for integrated optics," *Nanophotonics*, vol. 3, no. 4–5, pp. 205–214, Jan. 2014, doi: 10.1515/nanoph-2013-0034.

[3] A. Rahim *et al.*, "Expanding the silicon photonics portfolio with silicon nitride photonic integrated circuits," *J. Lightw. Technol.*, vol. 35, no. 4, pp. 639–649, Feb. 2017, doi: 10.1109/JLT.2016.2617624.

[4] K. Okamoto, "Recent progress of integrated optics planar lightwave circuits," *Opt. Quantum Electron.*, vol. 31, no. 2, pp. 107–129, Feb. 1999, doi: 10.1023/A:1006975415469.

[5] A. Boes, B. Corcoran, L. Chang, J. Bowers, and A. Mitchell, "Status and potential of lithium niobate on insulator (LNOI) for photonic integrated circuits," *Laser Photon. Rev.*, vol. 12, no. 4, Apr. 2018, Art. no. 1700256, doi: 10.1002/lpor.201700256.

[6] X.-Y. Han *et al.*, "Recent progress of imprinted polymer photonic waveguide devices and applications," *Polymers*, vol. 10, no. 6, Art. no. 603, Jun. 2018, doi: 10.3390/polym10060603.

[7] Y. Jiao *et al.*, "InP membrane integrated photonics research," *Semicond. Sci. Technol.*, vol. 36, no. 1, Jan. 2020, Art. no. 013001, doi: 10.1088/1361-6641/abcadd.

[8] W. Bogaerts *et al.*, "Compact wavelength-selective functions in Silicon-on-Insulator photonic wires," *IEEE J. Sel. Topics Quantum Electron.*, vol. 12, no. 6, pp. 1394–1401, Nov. 2006, doi: 10.1109/JSTQE.2006.884088.

[9] W. Song *et al.*, "High-density waveguide superlattices with low crosstalk," *Nat. Commun.*, vol. 6, no. 1, Nov. 2015, Art. no. 7027, doi: 10.1038/ncomms8027.

[10] Y. Su, Y. Zhang, C. Qiu, X. Guo, and L. Sun, "Silicon photonic platform for passive waveguide devices: Materials, fabrication, and applications," *Adv. Mater. Technol.*, vol. 5, no. 8, Aug. 2020, Art. no. 1901153, doi: 10.1002/admt.201901153.

[11] R. Gatdula, S. Abbaslou, M. Lu, A. Stein, and W. Jiang, "Guiding light in bent waveguide superlattices with low crosstalk," *Optica*, vol. 6, no. 5, May 2019, Art. no. 585, doi: 10.1364/OPTICA.6.000585.

[12] Y. Yang *et al.*, "Crosstalk reduction of integrated optical waveguides with nonuniform subwavelength silicon strips," *Sci. Rep.*, vol. 10, no. 1, Dec. 2020, Art. no. 4491, doi: 10.1038/s41598-020-61149-1.

[13] S. Jahani and Z. Jacob, "All-dielectric metamaterials," *Nat. Nanotechnol.*, vol. 11, no. 1, pp. 23–36, Jan. 2016, doi: 10.1038/nnano.2015.304.

[14] F. J. Rodríguez-Fortuño, A. Espinosa-Soria, and A. Martínez, "Exploiting metamaterials, plasmonics and nanoantennas concepts in silicon photonics," *J. Opt.*, vol. 18, no. 12, 2016, Art. no. 123001, doi: 10.1088/2040-8978/18/12/123001.

[15] P. Cheben, R. Halir, J. H. Schmid, H. A. Atwater, and D. R. Smith, "Subwavelength integrated photonics," *Nature*, vol. 560, no. 7720, Aug. 2018, Art. no. 565, doi: 10.1038/s41586-018-0421-7.

[16] P. J. Bock *et al.*, "Subwavelength grating periodic structures in silicon-on-insulator: A new type of microphotonic waveguide," *Opt. Exp.*, vol. 18, no. 19, pp. 20251–20262, Sep. 2010, doi: 10.1364/OE.18.020251.

[17] R. Halir *et al.*, "Subwavelength-grating metamaterial structures for silicon photonic devices," *Proc. IEEE*, vol. 106, no. 12, pp. 2144–2157, Dec. 2018, doi: 10.1109/JPROC.2018.2851614.

[18] A. Martínez, "Integration of subwavelength nanostructures in silicon waveguides: New phenomena and applications," in *MetamaterialsX. I.*, vol. 10671, May 2018, Art. no. 106711Y, doi: 10.1117/12.2305489.

[19] L. Sun, Y. Zhang, Y. He, H. Wang, and Y. Su, "Subwavelength structured silicon waveguides and photonic devices," *Nanophotonics*, vol. 9, no. 6, pp. 1321–1340, May 2020, doi: 10.1515/nanoph-2020-0070.

[20] K. Bi, Q. Wang, J. Xu, L. Chen, C. Lan, and M. Lei, "All-dielectric metamaterial fabrication techniques," *Adv. Opt. Mater.*, vol. 9, no. 1, 2021, Art. no. 2001474, doi: https://doi.org/10.1002/adom.202001474.

[21] S. Berthier and J. Lafait, "Effective medium theory: Mathematical determination of the physical solution for the dielectric constant," *Opt. Commun.*, vol. 33, no. 3, pp. 303–306, Jun. 1980, doi: 10.1016/0030-4018(80)90249-7.

[22] D. Benedikovic *et al.*, "Subwavelength index engineered surface grating coupler with sub-decibel efficiency for 220-nm silicon-on-insulator waveguides," *Opt. Exp.*, vol. 23, no. 17, pp. 22628–22635, Aug. 2015, doi: 10.1364/OE.23.022628.

[23] X. Mu, S. Wu, L. Cheng, and H. Y. Fu, "Edge couplers in silicon photonic integrated circuits: A review," *Appl. Sci.*, vol. 10, no. 4, Feb. 2020, Art. no. 1538, doi: 10.3390/app10041538.

[24] Y. Wang *et al.*, "Compact broadband directional couplers using subwavelength gratings," *IEEE Photon. J.*, vol. 8, no. 3, Jun. 2016, Art. no. 7101408, doi: 10.1109/JPHOT.2016.2574335.

[25] Y. Zhang *et al.*, "On-chip silicon polarization and mode handling devices," *Front. Optoelectron.*, vol. 11, no. 1, pp. 77–91, Mar. 2018, doi: 10.1007/s12200-018-0772-6.

[26] H. Wu, C. Li, L. Song, H.-K. Tsang, J. E. Bowers, and D. Dai, "Ultra-sharp multimode waveguide bends with subwavelength gratings," *Laser Photon. Rev.*, vol. 13, no. 2, Feb. 2019, Art. no. 1800119, doi: 10.1002/lpor.201800119.

[27] L. Huang *et al.*, "Improving the detection limit for on-chip photonic sensors based on subwavelength grating racetrack resonators," *Opt. Exp.*, vol. 25, no. 9, pp. 10527–10535, May 2017, doi: 10.1364/OE.25.010527.

[28] S. Jahani *et al.*, "Controlling evanescent waves using silicon photonic all-dielectric metamaterials for dense integration," *Nat. Commun.*, vol. 9, May 2018, Art. no. 1893, doi: 10.1038/s41467-018-04276-8.

[29] S. Jahani and Z. Jacob, "Photonic skin-depth engineering," *J. Opt. Soc. Amer. B*, vol. 32, no. 7, Jul. 2015, Art. no. 1346, doi: 10.1364/JOSAB.32.001346.

[30] S. Jahani and Z. Jacob, "Transparent sub-diffraction optics: Nanoscale light confinement without metal," in *Proc. IEEE Photon. Conf.*, 2014, Art. no. 15.

[31] A. Debevc, J. Krč, and M. Topič, "Design of silicon waveguides with all-dielectric metamaterial cladding by employing numerical simulations," in *Metamaterials XII*, vol. 11344, Apr. 2020, Art. no. 1134420. doi: 10.1117/12.2555854.

[32] Y. Bian, Q. Ren, L. Kang, Y. Qin, P. L. Werner, and D. H. Werner, "Efficient cross-talk reduction of nanophotonic circuits enabled by fabrication friendly periodic silicon strip arrays," *Sci. Reps.*, vol. 7, no. 1, Dec. 2017, doi: 10.1038/s41598-017-16096-9.

[33] M. B. Mia, S. Z. Ahmed, I. Ahmed, Y. J. Lee, M. Qi, and S. Kim, "Exceptional coupling in photonic anisotropic metamaterials for extremely low waveguide crosstalk," *Optica*, vol. 7, no. 8, pp. 881, Aug. 2020, doi: 10.1364/OPTICA.394987.

[34] N. Kumar, M. R. Shenoy, K. Thyagarajan, and B. P. Pal, "Graphical representation of the supermode theory of a waveguide directional coupler," *Fiber Integr. Opt.*, vol. 25, no. 3, pp. 231–244, Jul. 2006, doi: 10.1080/01468030600569925.

[35] L. Wang *et al.*, "Design of a low-crosstalk half-wavelength pitch nano-structured silicon waveguide array," *Opt. Lett.*, vol. 44, no. 13, pp. 3266–3269, Jul. 2019, doi: 10.1364/OL.44.003266.

[36] K. E. Oughstun and N. A. Cartwright, "On the lorentz-lorenz formula and the lorentz model of dielectric dispersion," *Opt. Exp.*, vol. 11, no. 13, pp. 1541–1546, Jun. 2003, doi: 10.1364/OE.11.001541.

[37] "COMSOL: Multiphysics software for optimizing designs," *COMSOL*. Accessed: Jun. 10, 2021. [Online]. Available: https://www.comsol.com/

[38] P. Pintus *et al.*, "PWM-driven thermally tunable silicon microring resonators: Design, fabrication, and characterization," *Laser Photon. Rev.*, vol. 13, no. 9, Art. no. 1800275, Sep. 2019, doi: 10.1002/lpor.201800275.

[39] S. K. Selvaraja, W. Bogaerts, P. Dumon, D. Van Thourhout, and R. Baets, "Subnanometer linewidth uniformity in silicon nanophotonic waveguide devices using CMOS fabrication technology," *IEEE J. Sel. Topics Quantum Electron.*, vol. 16, no. 1, pp. 316–324, Jan. 2010, doi: 10.1109/JSTQE.2009.2026550.